Near-Infrared Emission by Tuned Aggregation of a Porphyrin Compound in a Host–Guest Light-Emitting Electrochemical Cell

ADVANCED OPTICAL MATERIALS
www.advopticalmat.de

Near-Infrared Emission by Tuned Aggregation of a Porphyrin Compound in a Host–Guest Light-Emitting Electrochemical Cell

Mariza Mone, Shi Tang, Zewdneh Genene, Petri Murto, Martyn Jevric, Xianshao Zou, Joan Ràfols-Ribé, Birhan A. Abdulahi, Jia Wang, Wendimagegn Mammo, Mats R. Andersson, Ludvig Edman,* and Ergang Wang**

The synthesis of 5,10,15,20-tetrakis((5,10-bis((2-hexyldecyl)oxy)dithieno[3,2-*c*:3′,2′-*h*][1,5]naphthyridin-2-yl)ethynyl)porphyrin zinc(II) (Por4NT), a near-infrared (NIR) emitting compound, comprising a zinc porphyrin core linked with triple bonds through its *meso* positions to four 5,10-bis((2-hexyldecyl) oxy)dithieno[3,2-*c*:3′,2′-*h*][1,5]naphthyridine (NT) arms is reported. Por4NT featured high solubility in common non-polar solvents, which is ideal for easy processing through solution techniques, and high photoluminescence (PL) efficiency of ≈30% in dilute toluene solution. It also exhibited a strong tendency for aggregation because of its flat conformation, and this aggregation resulted in a strong redshifted emission and a drop in PL efficiency. A well-matched PBDTSi-BDD-Py "host" terpolymer is therefore designed, which is capable of mitigating the aggregation of the Por4NT "guest". An optimized blend of the host, guest, and an ionic-liquid electrolyte is utilized as the active material in a light-emitting electrochemical cell (LEC), which delivered strong NIR radiance of 134 μW cm^{-2} with a long wavelength maximum at 810 nm at a low drive voltage of 5.0 V. The attainment of the strong NIR emission from the host–guest LEC is attributed to a tuned aggregation of the Por4NT emitter, which resulted in the desired aggregation-induced redshift of the emission at a reasonably retained efficiency.

1. Introduction

Materials that emit in the near-infrared (NIR) range are critical for the realization of a wide range of applications in, for example, optical communication, security authentication, and medicine,[1] with the latter applications in part effectuated by the NIR window between 700–1000 nm of biological tissue.[2] Soluble organic NIR emitters are of particular interest for such applications since they can allow for cost-efficient solution-based fabrication of flexible devices.[3] However, organic NIR emitters have a drawback because they typically exhibit a significantly lower emission efficiency than the corresponding visible emitters,[2] because of the so-called energy-gap law and their tendency to aggregate into low-emissive H-aggregates.[4] The energy-gap law states that the probability of non-radiative transitions increases with increasing wavelength (decreasing energy), due to a concomitant increase in overlap

Dr. M. Mone, Dr. Z. Genene, Dr. B. A. Abdulahi, Prof. E. Wang
Chalmers University of Technology
Göteborg SE-412 96, Sweden
E-mail: ergang@chalmers.se
Dr. S. Tang, Dr. J. Ràfols-Ribé, Dr. J. Wang, Prof. L. Edman
Umeå University
Umeå SE-90187, Sweden
E-mail: ludvig.edman@umu.se
Dr. Z. Genene
Ambo University
P.O. Box 19, Addis Ababa, Ethiopia
The ORCID identification number(s) for the author(s) of this article can be found under https://doi.org/10.1002/adom.202001701.

DOI: 10.1002/adom.202001701

Dr. P. Murto
University of Cambridge
Cambridge CB2 1EW, UK
Dr. M. Jevric, Prof. M. R. Andersson
Flinders University
Sturt Road, Bedford Park, Adelaide, South Australia 5042, Australia
E-mail: mats.andersson@flinders.edu.au
Dr. X. Zou
Division of Chemical Physics
Lund University
Box 124, Lund 221 00, Sweden
Dr. B. A. Abdulahi
Wollo University
P.O. Box 19, Dessie, Ethiopia
Dr. Z. Genene, Dr. B. A. Abdulahi, Prof. W. Mammo
Addis Ababa University
P.O. Box, Addis Ababa 33658, Ethiopia
Prof. E. Wang
Zhengzhou University
Zhengzhou 450001, China

between the lower vibrational levels of the emissive first excited singlet/triplet state (S_1/T_1) with the higher vibrational levels of the singlet ground state (S_0).[5] The formation of face-to-face H-aggregates results in the creation of two excited states with different energies, with the probability of radiative transition from the lower-energy state being very low.[4,6] A practical approach to mitigate the issues pertaining to aggregation and to improve the emission efficiency is to disperse the emitter in a host matrix.[7]

Two devices that utilize organic emitters for the practical electroluminescent (i.e., "cold" emission) conversion of electric current to light emission are the organic light-emitting diode (OLED) and the light-emitting electrochemical cell (LEC). The LEC is distinguished from the OLED by the existence of mobile ions in the active material, which allow for in situ electrochemical doping of the electroactive compound (often the emitter) during operation. This process eventually results in the formation of a light-emitting p–n junction in the active material.[8] This particular LEC operation is of interest since it has paved the way for the fabrication of light-weight,[9] flexible,[10] stretchable,[11] fiber-shaped,[12] and large-area LEC devices[13] at very low-cost[14] using scalable printing and coating methods.[10b–d,13a,15] Recently, it was also demonstrated that well-designed host–guest LEC devices can deliver strong luminance at high efficiency.[16]

A recent review by Pilkington et al.[19] nicely summarized the current status of NIR-emitting LEC devices. The majority of NIR-emitting LECs to date comprise ionic transition metal complexes (iTMCs) based on Ru[17] and Ir[7c] as the emitter, although NIR-emitting LECs based on Os[18] have also been reported. In 2008, Xun et al.[20] reported a series of Ru-based NIR emitters, which delivered long-wavelength NIR emission at ≈880–900 nm in LEC devices, but which also suffered from a low peak radiance of < 10 μW cm^{-2}. Ho and co-workers[21] employed an Ir complex and a laser dye in a host–guest LEC, but this device also delivered a very low radiance output of <10 μW cm^{-2}. More recently a set of NIR-LECs comprising Ir-based iTMCs as the emitter was reported, which featured NIR emission from excimers. These devices exhibited high radiance (143–303 μW cm^{-2}) and EQE (0.26–0.57%) for an EL peak wavelength >800 nm.[22] However, for many applications, it is preferable to employ emitters that are free from expensive and rare metals in the Pt group,[23] and in this context Pertegas et al.[24] reported LECs comprising two cyanine dyes as the host–guest blend, which featured a radiance of 170 μW cm^{-2} at a peak wavelength of ≈700 nm and an EQE of 0.44%. Tang and coworkers[25] reported the synthesis of a donor-acceptor copolymer, which was employed as the single-emitter in a NIR-LEC that delivered a radiance of 129 μW cm^{-2} at a peak wavelength of 705 nm and a low drive voltage of 3.4 V. Finally, Murto et al.[13b] incorporated a set of designed polymeric emitters in host–guest LECs, which exhibited a high radiance of 1500 μW cm^{-2} at a peak wavelength of 725 nm.

Porphyrins are organic compounds employed by nature for a number of different tasks, notably for photosynthesis[26] and for oxygen transport in the blood stream.[27] They have also been employed as emitters in OLEDs.[28] The optical properties of porphyrins can be modified to achieve emission in the NIR region via the selection of the central metal atom and by the modification of the chemical constituents attached to the *meso* and *β* positions of the porphyrin core.[4,29] Recently, we reported the synthesis of a star-shaped diketopyrrolopyrrole-substituted Zn porphyrin that delivered deep NIR emission with a peak wavelength of 900 nm when introduced in an LEC device. However, the peak radiance and the external quantum efficiency (EQE) attained were quite low at 36 μW cm^{-2} and 0.028%, respectively.[30]

In this work, we report the synthesis and characterization of a NIR emissive 5,10,15,20-tetrakis((5,10-bis((2-hexyldecyl)oxy)dithieno[3,2-*c*:3′,2′-*h*][1,5]naphthyridin-2-yl)ethynyl)porphyrin zinc(II) (Por4NT) and a compatible conjugated polymer (PBDTSi-BDD-Py) with a well-matched larger energy-gap. Through systematic experimentation and modeling, we established that Por4NT has a strong tendency to form aggregates in both solution and in the solid-state, and that this aggregation is manifested in a strong redshift and decreased efficiency of the emission. However, we found that PBDTSi-BDD-Py is capable of efficiently alleviating this aggregation, in particular, because of the introduced pyridine moiety in its backbone. By optimizing a Por4NT:PBDTSi-BDD-Py:electrolyte blend for the active material in an LEC device, we obtained a strong NIR radiance of 134 μW cm^{-2} (peak wavelength = 810 nm) with an EQE of 0.121% at a low drive voltage of 5.0 V.

2. Results and Discussion

Figure 1 presents the chemical structure of the guest emitter, Por4NT, which consists of a zinc porphyrin core connected to four 5,10-bis((2-hexyldecyl)oxy)dithieno[3,2-*c*:3',2'-*h*][1,5]naphthyridine (NT) units via acetylenic bonds at its *meso* positions. Zn was selected as the porphyrin core metal over, e. g., Pt or Pd, because of its abundance, low toxicity, and low price.[31] The choice of the large fused tetracyclic NT ring moiety was motivated by its extended conjugation and planarity, which was anticipated to result in redshifted emission, significant solid-state packing, and high charge-carrier mobility. Each NT unit was further decorated with two long and branched (2-hexyldecyl)oxy side chains to endow the porphyrin compound with high solubility in common organic solvents for facile solution processing. Thermogravimetric analysis (TGA) and differential scanning calorimetry (DSC) of solid Por4NT (Figure S1, Supporting Information) revealed a high decomposition temperature of 300 °C under inert atmosphere, and no thermal transition between −50 and 250 °C.

Scheme S1, Supporting Information, shows the synthesis of the NT monobromide units following the procedure outlined by Kroon *et al.* [32] The porphyrin core of the guest emitter, Por4NT, was synthesized by condensation of 3-(triisopropylsilyl) propiolaldehyde with pyrrole followed by oxidation as described by Lindsey.[33] The porphyrin core was further metallated by reaction with zinc acetate dihydrate to afford ZnP-TIPS$_4$.[30] Desilylation of ZnP-TIPS$_4$ with TBAF followed by Sonogashira coupling of the intermediate with NT monobromide afforded Por4NT, as depicted in Scheme S2, Supporting Information.

Figure 1 shows the chemical structures of the three host polymers, poly[(4,8-bis(5-(tributylsilyl)thiophen-2-yl)benzo[1,2-*b*:4,5-*b*′]dithiophene-2,6-diyl-*alt*-(5,5-(1′,3′-di-2-thienyl-5′,7′-bis(2-ethylhexyl)benzo[1′,2′-*c*:4′,5′-*c*′]dithiophene-4,8-dione)] (PBDTSi-BDD), PBDTSi-BDD-Py and poly[(9,9-di-n-octylfluorenyl-2,7-diyl)-*alt*-(benzo[2,1,3]thiadiazol-4,8-diyl)] (F8BT). Recently,

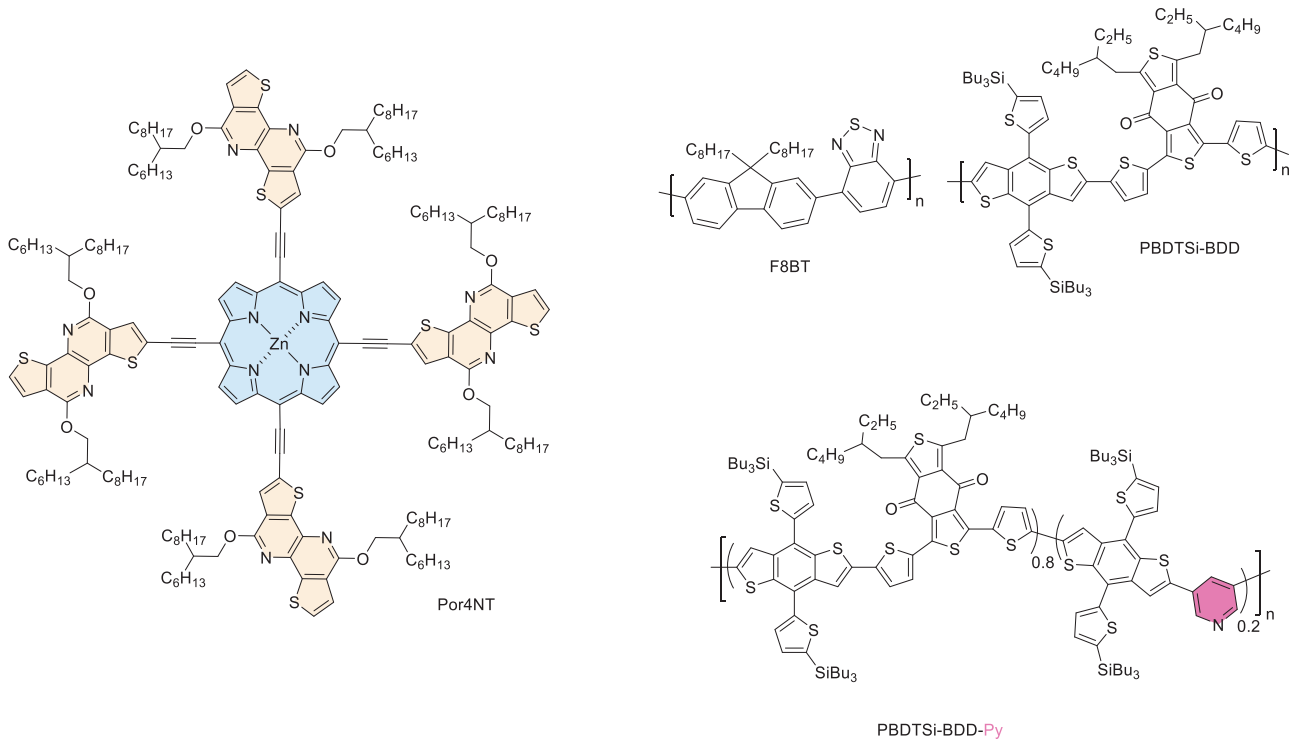

Figure 1. The chemical structure of the Por4NT guest emitter and the three host polymers, F8BT, PBDTSi-BDD, and PBDTSi-BDD-Py.

we reported the design, synthesis, and functional application of PBDTSi-BDD.[30] PBDTSi-BDD-Py was prepared by the replacement of 20% of the 1,3-bis(5-bromothiophen-2-yl)-5,7-bis(2-ethylhexyl)-4*H*,8*H*-benzo[1,2-*c*:4,5-*c*′]dithiophene-4,8-dione (BDD) moieties in PBDTSi-BDD with pyridine units. The presence of pyridine units in PBDTSi-BDD-Py terpolymer was expected to facilitate axial coordination to the zinc metal core of Por4NT through the lone pair of electrons on the nitrogen atom leading to improved solubility and dispersity of the guest in the host matrix.[34] In addition, pyridine derivatives are commonly good electron transport materials because of their electron-withdrawing nature.[35] Moreover, the presence of pyridine reduces the polymer regularity and thereby renders the polymer backbone more flexible, which is expected to allow for more facile ion migration and electrochemical doping in the active material during LEC operation.[36] The third host polymer, F8BT, was included in this study because it is a common benchmark host material that is frequently employed in high-performance host–guest light-emitting devices.[37]

The host polymer PBDTSi-BDD-Py was synthesized by the Stille coupling reaction between ((2,6-bis(trimethylstannyl) benzo[1,2-*b*:4,5-*b*′]dithiophene-4,8-diyl)bis(thiophene-5,2-diyl)) bis(tributyl-silane) (BDTSi-Sn_2), 1,3-bis(5-bromothiophen-2-yl)-5,7-bis(2-ethylhexyl)-4*H*,8*H*-benzo[1,2-*c*:4,5-*c*′]dithiophene-4,8-dione (BDD-Br_2) and 3,5-dibromopyridine (Py-Br_2) in the ratio of 1.0:0.8:0.2 as illustrated in Scheme S3. The number average molecular weight of PBDTSi-BDD-Py was 20.8 kDa with a polydispersity index of 2.03 as determined by gel permeation chromatography. TGA and DSC studies of both PBDTSi-BDD-Py and PBDTSi-BDD (Figure S1, Supporting Information) revealed that both polymers exhibit desired high decomposition temperatures close to 400 °C under inert atmosphere without thermal transitions between −50 and 250 °C.

Density functional theory (DFT) calculations were employed to study the molecular conformations and the electronic transitions of Por4NT. **Figure 2**a presents a side-view (upper part) and top-view (lower part) of the ground-state conformation (S_0, red structure) and the first-excited-state conformation (S_1, green structure) of Por4NT. The DFT data reveal that Por4NT adopts a highly coplanar conformation in both the ground state and the excited state. The modeling was performed with isobutoxy side chains of a C_{4h} point group conformation, but the complementary systematic DFT study presented in Figures S2 and S3 shows that the detailed conformation (C_{4h} and D_{2h} point groups) and the exact length of the side chains (methoxy, isobutoxy, 2-ethylbutoxy and 2-propylpentyloxy) have a negligible influence on the optimized ground state conformation and the excited state energy.

Figure 2b presents the DFT-calculated natural transition orbitals (NTOs) of the lowest-energy electronic transition. We find that the hole and the electron distribution are both localized at the center part of the molecule, and that they are strongly overlapping in space. It is thus anticipated that the localized excited state is effectively protected from the surrounding by the bulky side chains, which in turn is expected to lead to a high yield of emissive excitons.[38] This hypothesis is further supported by the observation that the highest occupied molecular orbital (HOMO) and the lowest unoccupied molecular orbital (LUMO) distributions in the ground state were also calculated to be co-localized at the central part of the molecule (Figure S4, Supporting Information). The DFT further predicted that the vertical excitation energy of Por4NT is

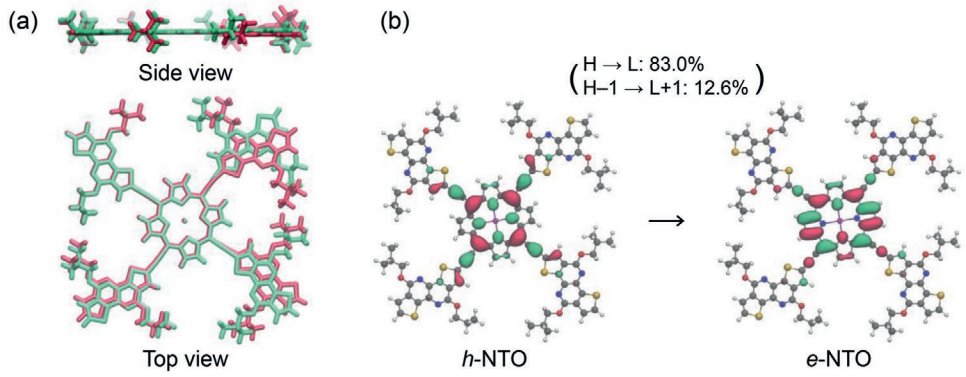

Figure 2. a) Side-view and top-view conformation of Por4NT in the geometry-optimized ground state (S_0, red structure) and the lowest-energy excited state (S_1, green structure). b) The natural transition orbitals for the S_1 state, with *h* representing the hole distribution and *e* the electron distribution. The corresponding contributions of the principal molecular orbitals to the transitions are shown in parenthesis (H = HOMO, L = LUMO).

1.92 eV, and that the energy of the geometry-optimized S_1 state, that is, the adiabatic excitation energy is 1.78 eV.

Figure 3a presents the absorption spectrum of the Por4NT emitter at different concentrations in toluene solution and as a thin film. Por4NT exhibited two absorption maxima at ≈515 nm and ≈705 nm (see **Table 1**), which are attributed to the S_0-S_2 ("the Soret band") and the S_0-S_1 ("the Q band") transitions, respectively.[39] We find that the Soret band is slightly blue-shifted with increasing Por4NT concentration, while the Q-band is slightly redshifted. In the solid Por4NT film, the Soret band peaked at 495 nm and the Q band at 724 nm. The optical energy gap of Por4NT was calculated from the onset of absorption in the solid-state to be 1.61 eV. Figure S5a, Supporting Information, presents a plot of the absolute value of the molar extinction coefficient of the Por4NT solution as a function of wavelength, and it peaked at a high value of $\approx 5 \times 10^5$ M^{-1} cm^{-1} in the Soret band region and reached $\approx 1 \times 10^5$ M^{-1} cm^{-1} in the Q band region.

Figure 3b displays the normalized photoluminescence (PL) spectrum of Por4NT at concentrations ranging from 1×10^{-7} M to 1×10^{-4} M in toluene. Two PL peaks at ≈730–740 nm and ≈810–820 nm are observed for all concentrations, but the relative intensity of the longer-wavelength peak increases strongly with the Por4NT concentration. We also note that the longer-wavelength peak is redshifted somewhat with increasing concentration from 809 nm at 1×10^{-7} M to 823 nm at 1×10^{-4} M. A comparison with the absorption data in Figure 3a reveals that the Stokes shift of the S_0-S_1 transition is low at ≈20 nm (=44 meV). Table 1 further reveals that the PL quantum yield (PLQY) drops significantly with increasing Por4NT concentration from 29.3% at 1×10^{-7} M to 3.8% at 1×10^{-4} M. Notably, we could not detect any measurable PL from the solid Por4NT film.

Our observations from the emission studies suggest that Por4NT has a strong propensity for aggregation both in solution and in the solid-state.[40] This behavior is in agreement with the conformational DFT results depicted in Figure 2a, which revealed that Por4NT prefers to adopt a highly flat conformation in both the ground state and the excited state. Accordingly, we suggest that the aggregation of Por4NT takes the form of flat-on packing. We thus assign the higher-energy PL peak at ≈730–740 nm to the emission from "aggregation-free Por4NT" molecules, and the lower-energy PL peak at ≈810–820 nm to "partially aggregated Por4NT" molecules. It is worth noting that solid films of the "fully aggregated Por4NT" molecules do not exhibit measurable PL. We also note that the comparatively concentration-invariant absorption (Figure 3a) suggests that the influence of aggregation is most prominent in the emission.

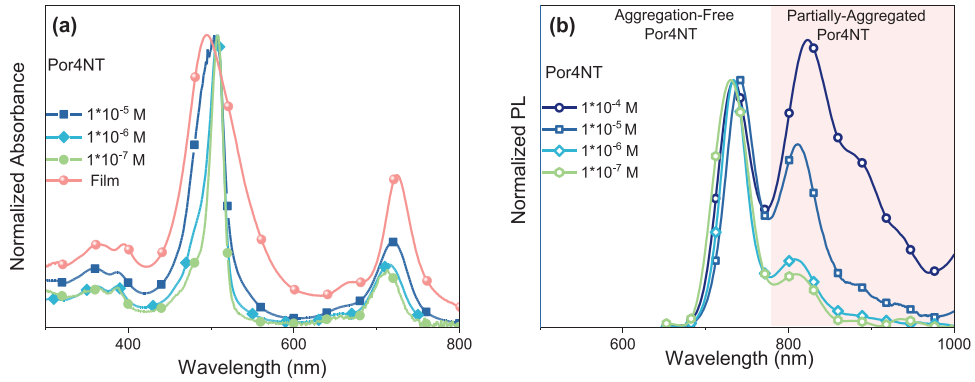

Figure 3. a) Normalized absorption spectra of the Por4NT guest in toluene solution at different concentrations and as a thin film on a glass substrate. b) The room temperature normalized PL spectra of the Por4NT guest in toluene solution at different concentrations. The first peak is marked as "aggregation-free Por4NT" and the second as "partially aggregated Por4NT". No PL emission could be detected from the solid Por4NT film.

Table 1. Optical properties of the Por4NT emitter as a function of concentration in toluene solution and as a thin film.

Concentration [M]	Soret-band absorption peak [nm]	Q-band absorption peak [nm]	PL peaks [nm]	PLQY [%]
10^{-7}	508	714	730, 809	29.3
10^{-6}	508	714	733, 806	25.4
10^{-5}	504	719	741, 811	12.8
10^{-4}	N/A	N/A	733, 823	3.8
Film	495	724	N/A	N/A

The three host polymers were optically characterized as regards to their capacity to function as efficient hosts for the Por4NT guest. Figure S5b, Supporting Information, presents the normalized absorption spectra of thin films of the host polymers which show absorption maxima at 465, 600, and 560 nm for F8BT, PBDTSi-BDD, and PBDTSi-BDD-Py, respectively. The optical energy gap, as derived from the onset of absorption, is 2.32 eV for F8BT, 1.83 eV for PBDTSi-BDD, and 1.84 eV for PBDTSi-BDD-Py. **Figure 4**a presents the normalized PL spectra of the three host polymers and the absorption spectrum of the Por4NT guest emitter. F8BT exhibited the highest-energy emission with the PL peak at 558 nm. PBDTSi-BDD featured the lowest-energy emission with its PL peak at 748 nm, whereas the PL peak of PBDTSi-BDD-Py is positioned at 690 nm. The solid-state PLQY was measured to be 4.1% for F8BT, 5.2% for PBDTSi-BDD, and 7.6% for PBDTSi-BDD-Py. The incorporation of the pyridine moiety in the backbone of the terpolymer PBDTSi-BDD-Py resulted in a significant blueshift of both the absorption and the emission, as well as an increase in the PL efficiency, in comparison to the copolymer PBDTSi-BDD. Time-resolved PL (TRPL) measurements were also conducted with an excitation wavelength of 400 nm, and the lifetimes (τ) of the neat host films and the host–guest blend films with a guest concentration of 7 mass% were measured. The normalized spectra are presented in Figure S8, Supporting Information, and the lifetime was estimated by the 1/e method, considering the instrumental response function. Table S2, Supporting Information, presents the derived rates of the radiative and the non-radiative processes using the values for the PLQY and the PL lifetimes. Note that the non-radiative processes in blend polymers can include a carrier dissociation processes after the photogeneration. The TRPL data show that the neat host films exhibit very short lifetimes on the order of picoseconds, and that the lifetime is even shorter for the blend films. This indicates that the energy transfer process from host to guest is very fast. It also confirms that the emission is in the form of short-lived fluorescence and not long-lived phosphorescence.

Importantly, we find that the PL spectrum of F8BT exhibits a partial overlap with the higher-energy Soret-band absorption of the Por4NT guest emitter, whereas the PL spectra of PBDTSi-BDD and PBDTSi-BDD-Py feature almost perfect overlap with the lower-energy Q-band absorption of Por4NT. This observation indicates that efficient Förster resonance energy transfer from host to guest can take place for all three host–guest blends. A more direct investigation of the merits for host-to-guest energy transfer is provided by Figure 4b, which presents the PL spectra of thin films of the host–guest blends. With F8BT as the host polymer, two significant PL peaks are observed, with the one at 560 nm being due to the F8BT host and the one at 821 nm originating from the Por4NT guest; this shows that the host to guest energy transfer for the F8BT system is not complete. A more complete host to guest energy transfer is observed for the other two host–guest systems, with the major PL peak being positioned at 820 and 817 nm for PBDTSi-BDD:Por4NT and PBDTSi-BDD-Py:Por4NT blends, respectively. This majority

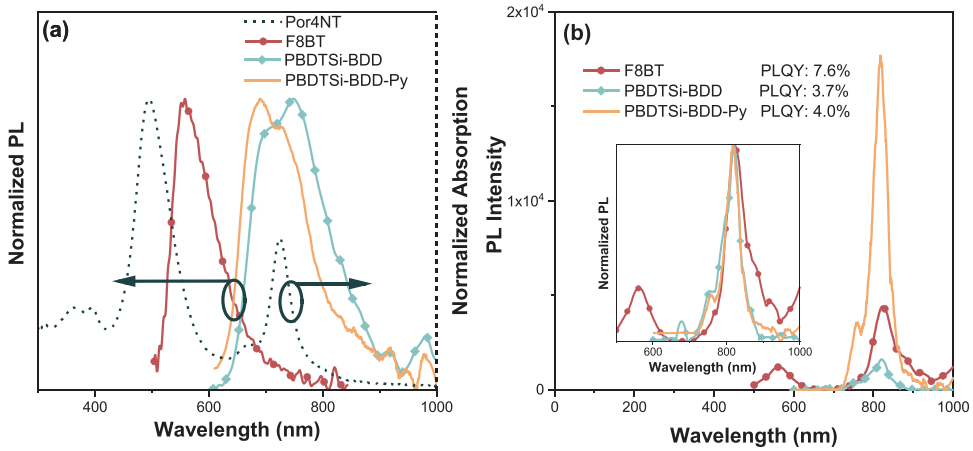

Figure 4. a) The absorption spectrum of the Por4NT guest (dashed black line, right y-axis) and the normalized PL spectra of the three host polymers (left y-axis). b) The non-normalized PL spectrum of thin films of the host–guest blends with a guest concentration of 7%, with the inset showing the corresponding normalized PL spectrum. The absorption and PL data are recorded on thin films on quartz substrates at room temperature.

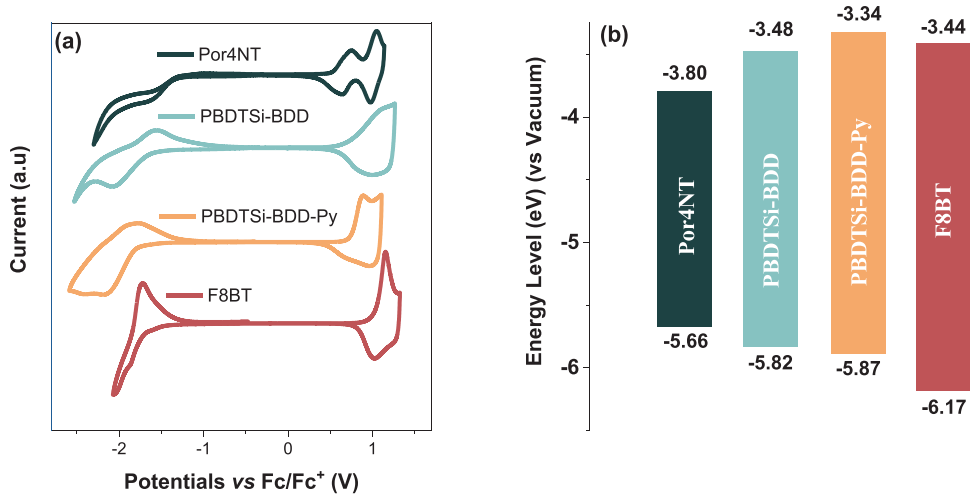

Figure 5. a) The CV traces of the three host polymers and the Por4NT guest emitter. b) The energy levels of the three host polymers and the Por4NT guest emitter derived from CV. The CV data are measured on solid thin films deposited on a Pt wire as the working electrode, and the scan speed is 100 mV s^{-1}.

peak originates from the Por4NT guest emitter, while only a very weak remnant higher-energy PL emission is observed from the host. More specifically, for the PBDTSi-BDD:Por4NT blend the remnant host PL corresponded to ≈15% of the total PL, while for the PBDTSi-BDD-Py:Por4NT it was even lower at ≈11%. Finally, we also measured the solid-state PLQY of the host–guest blends, and it was 7.6% for F8BT:Por4NT, 3.7% for PBDTSi-BDD:Por4NT, and 4.0% for PBDTSi-BDD-Py.

The electrochemical properties of the three host polymers and the Por4NT guest molecule are critical for the operation of LEC devices, and they were investigated by cyclic voltammetry (CV). **Figure 5**a shows the CV traces recorded on solid-state thin films, which reveal that all three host polymers exhibit highly reversible electrochemical oxidation and reduction reactions. The CV trace for the Por4NT guest indicates a highly reversible oxidation reaction, whereas the reduction reaction is less reversible, presumably because the reduced Por4NT is highly reactive in the CV solution.[41] We tentatively assigned the observed oxidation and reduction reactions to the conductivity-enhancing processes of p-type doping and n-type doping, respectively, and more support for this assignment is given below.

The HOMO and LUMO energy levels could be estimated from the measured onset potentials for oxidation (E_{ox}) and reduction (E_{red}) in CV, using the equations HOMO = $-(E_{ox} + 5.13)$ eV and LUMO = $-(E_{red} + 5.13)$ eV. Figure 5b presents a summary of the derived HOMO and LUMO levels, which are −5.66 and −3.80 eV, respectively, for the Por4NT guest. The electrochemical energy gap of Por4NT is accordingly 1.86 eV, which is higher than the measured optical gap of 1.61 eV. The derived HOMO values of the PBDTSi-BDD and PBDTSi-BDD-Py host polymers are −5.82 and −5.87 eV, while their LUMOs are positioned at −3.48 and −3.34 eV, respectively. The electrochemical energy gaps are 2.34 and 2.53 eV for PBDTSi-BDD and PBDTSi-BDD-Py, respectively, which are larger than their corresponding optical energy gaps of 1.83 and 1.84 eV, respectively. The LUMO level of F8BT is positioned in between that of the other two host polymers at −3.44 eV, whereas the HOMO is much deeper at −6.17 eV. This translates into the largest electrochemical energy gap of 2.73 eV for F8BT. We note that the energy levels of the Por4NT guest are located within the energy gap of all three host materials. This implies that both electrons and holes will be trapped on the Por4NT guest, which is beneficial for the host-to-guest energy transfer during electrical driving of host:guest blends in devices.[37a]

We now turn our attention to the performance of LEC devices based on the new host and guest materials. For the electrolyte in the active material, we selected to employ the ionic liquid tetrahexylammonium tetrafluoroborate ($THABF_4$, mass concentration = 5%), because of its broad electrochemical stability window is expected to inhibit non-desired electrolyte-induced side reactions.[42] The LEC devices were fabricated in an indium-tin-oxide (ITO)/poly(3,4-ethylenediophene):poly(styrenesulfonate) (PEDOT:PSS)/host:guest:$THABF_4$/Al configuration, and **Figures 6**a–c present the temporal evolution of such representative pristine devices with a) F8BT, b) PBDTSi-BDD, and c) PBDTSi-BDD-Py as the host polymer.

We find that all three device types feature a decreasing voltage and an increasing radiance during the initial operation at a constant current density of 75 mA cm^{-2}. This is the characteristic behavior of a well-behaved LEC device that features in situ conductivity- and injection-enhancing p-type and n-type doping at the two electrode interfaces,[43] and this observation thus yields further support to our previous conclusion that all three polymer hosts are functional LEC materials that can be both p- and n-type doped; see Figure 5 and related discussion. We note that the minimum drive voltage is lowest at 3.9 V with the host polymer being PBDTSi-BDD and highest at 6.9 V for the F8BT polymer, which is in agreement with that the electron/hole trap depths at the guest molecules are most shallow in the former system and deepest in the latter; see Figure 5b.

A comparison between the host-only devices (Por4NT concentration = 0%) and the host–guest devices in Figures 6d–f reveal that all host–guest LECs feature a significant emission contribution from the host polymer (at ≈550 nm for F8BT, ≈670 nm for PBDTSi-BDD, and ≈660 nm for PBDTSi-BDD-Py), but that this host contribution, as expected, is decreasing with

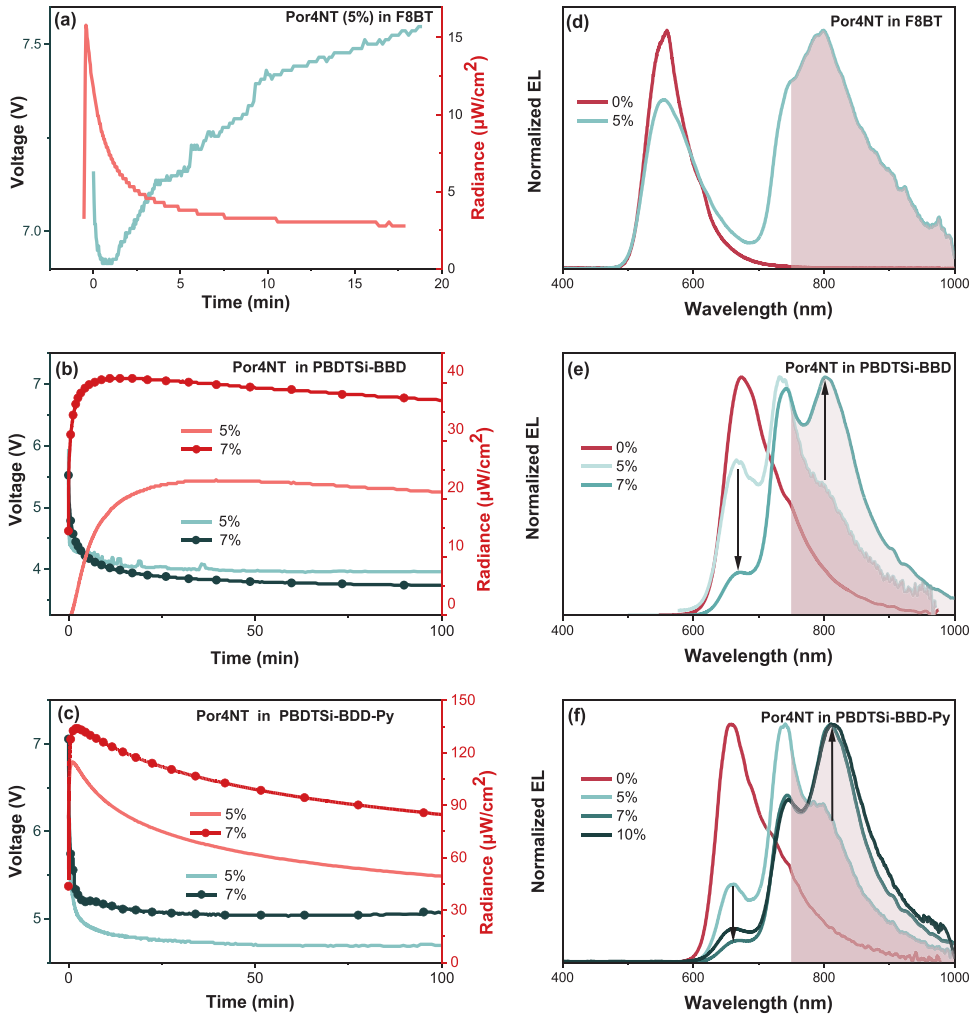

Figure 6. a–c) The temporal evolution of the voltage and radiance for the host–guest LECs comprising a) F8BT, b) PBDTSi-BDD, and c) PBDTSi-BDD-Py as the host. d–f) The steady-state EL spectra of host-only and host–guest LECs, with the host being d) F8BT, e) PBDTSi-BDD, and f) PBDTSi-BDD-Py. The arrows indicate improved host-to-guest energy transfer while the colored regions indicate the fraction of light emitted in the NIR regime >750 nm. The devices are driven by a current density of 75 mA cm^{-2}.

increasing Por4NT guest concentration. We also find that the overall NIR performance of the F8BT-NIR-LEC is inferior to that of the other two host–guest LECs (see also **Table 2**), and we therefore focused on the two new polymer hosts for the subsequent optimization and analysis.

This optimization resulted in that the best device performance was attained with a 7 mass% concentration of the Por4NT guest dispersed into the PBDTSi-BDD-Py host (and the $THABF_4$ electrolyte). More specifically, Table 2 shows that this device delivers a strong peak radiance of 134 μW cm^{-1} at an EQE of 0.121% and a drive voltage of 5.0 V. Importantly, a vast majority of this radiance (≈96%) is delivered in the NIR range above 700 nm, with the peak emission wavelength being 810 nm. Figure 6f shows that the fraction of NIR light is similar

Table 2. LEC performances as a function of host selection and guest concentration.

Host	Guest conc.	EL peaks [nm]	Peak radiance [μW cm^{-2}]	Lowest voltage [V]	EQE [%]	NIR fraction (>750 nm) [%]
F8BT	5%	550, 800	16	6.9	0.013	58
PBDTSi-BDD	5%	670, 735	23.1	3.9	0.019	47
PBDTSi-BDD-Py	5%	660, 740, 800	115	4.6	0.095	59
PBDTSi-BDD	7%	745, 802	40.7	3.6	0.037	73
PBDTSi-BDD-Py	7%	745, 810	134	5.0	0.121	80
PBDTSi-BDD-Py	10%	745, 810	33.5	7.9	0.03	80

for the Por4NT guest concentration of 10 mass%, but Table 2 reveals that the drawback is a significantly lowered radiance and efficiency and an increased voltage. The steady-state EL spectra of all of the host–guest LECs are displayed in Figure S7, Supporting Information.

The observation that the optimized PBDTSi-BDD-Py:Por4NT host–guest LEC emits efficient NIR light at 810 nm is interesting, since the PL data presented in Figures 3b and 4 strongly suggest that this emission originates from the "partially aggregated Por4NT" molecules. Remember that "fully aggregated Por4NT" molecules in a solid film do not feature any measurable emission in PL, and that isolated "free Por4NT" molecules emit at much shorter wavelengths. The device results also show that a Por4NT guest concentration above 7% results in a significant drop in radiance and efficiency, which suggests that the "partial aggregation"-"complete aggregation" threshold for good device performance is positioned at a guest concentration of 7%. Further support for this conclusion is provided by the AFM study displayed in Figure S9, Supporting Information, which shows that minor surface aggregation can be visibly observed in PBDTSi-BDD-Py:Por4NT active-material film at a Por4NT guest concentration of ≈7 mass%. We have also fabricated and characterized OLED devices, with PEDOT:PSS and Ca as the two electrodes, and Table S1, Supporting Information, show that the host–guest LECs outperform the corresponding host–guest OLEDs by a factor of two for both the peak radiance and the efficiency, while the drive voltage is essentially the same.

To summarize, we report on the design and synthesis of a new NIR porphyrin-based Por4NT emitter, which features a high solubility in common non-polar solvents and high PL efficiency of ≈30% in dilute toluene solution. Por4NT exhibits a strong tendency to form aggregates because of its flat conformation, and this aggregation results in a strong redshift, and a drop in efficiency of the emission. We therefore designed and synthesized a compatible PBDTSi-BDD-Py "host" terpolymer, which is capable of inhibiting the aggregation of the Por4NT "guest". An optimized blend of the host, guest and an ionic-liquid electrolyte was utilized as the active material in an LEC, and such optimized host–guest LECs delivered a strong NIR radiance of 134 μW cm^{-1} with a long peak wavelength of 810 nm at a low drive voltage of 5.0 V. We attribute the attainment of the strong NIR emission from the host–guest LEC to a tuned partial aggregation of the Por4NT emitter, which results in the desired aggregation-induced redshift of the emission at a reasonably retained efficiency. These results suggest that the future design of efficient porphyrin-based NIR emitters could consider a tuning of the aggregation through the introduction of bulky substituents at the porphyrine periphery and by a synthesis of emitter-compatible host materials.

3. Experimental Section

Material Characterization: Nuclear magnetic resonance spectra were recorded on a Bruker 600 MHz instrument in chloroform-d and pyridine-d5. For the host materials, size exclusion chromatography (SEC) was performed on an Agilent PL-GPC 220 integrated high-temperature GPC/SEC system with refractive index and viscometer detectors and three sequential PLgel 10 μm MIXED-B LS 300 × 7.5 mm columns. The eluent was 1,2,4-trichlorobenzene and the operating temperature was 150 °C. The molecular weights were calculated relative to calibration with polystyrene standards. The absorbance spectra were measured using a Varian Cary 50 UV/Vis spectrophotometer in a 10 × 10 mm^2 quartz cuvette. PL and PLQY measurements were carried out with a C9920 Hamamatsu absolute PLQY spectrometer. AFM measurements were performed in tapping mode using a MultiMode SPM microscope equipped with a Nanoscope IV Controller (Veeco Metrology) on solid-state thin films.TGA was conducted using a Mettler Toledo TGA/DSC 3+ STAR System under a N_2 atmosphere at a heating rate of 10 °C min^{-1}. DSC measurements were carried out on a Mettler Toledo DSC 2 STAR System under nitrogen atmosphere, over a temperature range of –80–380 °C using a heating/cooling rate of 10°C min^{-1} for PBDTSi-BDD, –80–350 °C for PBDTSi-BDD-Py and –80–300 °C for Por4NT.

Cyclic Voltammetry (CV): CV measurements were done on a CH-Instruments 650A Electrochemical Workstation in a three-electrode cell using a Pt wire as the working electrode, a Pt wire as the counter electrode, and a Ag wire as the quasi reference electrode calibrated using ferrocene/ferrocenium (Fc/Fc^+) redox couple. A 0.1 M tetrabutylammonium hexafluorophosphate (Bu_4NPF_6) in anhydrous acetonitrile solution was the electrolyte, which was bubbled with nitrogen before each measurement. The compound under study was deposited as a thin film onto the working electrode from a chloroform solution. The oxidation and reduction scans were measured separately at a scan rate of 100 mV s^{-1}, using a minimum of four measurements for each material to ensure repeatability. The HOMO and LUMO levels were derived from the first oxidation and reduction onset potential (E_{ox} and E_{red}) by setting the Fc/Fc^+ oxidation onset potential versus the normal hydrogen electrode (NHE) to 0.63 V and the NHE to –4.50 V in the Fermi vacuum scale using equations: HOMO = $-(E_{ox} + 5.13)$ eV and LUMO = $-(E_{red} + 5.13)$ eV.

Device Fabrication and Characterization: All materials were dissolved separately in anhydrous chlorobenzene. The concentration of the Por4NT guest was 10 mg mL^{-1} while that of the polymer hosts was 15 mg mL^{-1}. For the host–guest blends, the host-polymer, and the guest-emitter solutions were blended in the desired mass ratio. The active-material inks were prepared by adding tetrahexylammonium tetrafluoroborate ($THABF_4$) ionic liquid into host–guest blend at 5 mass%. The LEC devices were fabricated by sequentially spin-coating a poly(3,4-ethylenedioxythiophene):poly(styrene sulfonate) (PEDOT:PSS, Clevios P VP AI 4083, Heraeus) ink at 4000 rpm for 60 s and the active-material ink at 2000 rpm for 60 s onto carefully cleaned indium-tin-oxide (ITO) coated glass substrates (20 Ω per square, Thin Film Devices, US). The thickness of the dry PEDOT-PSS film was 40 nm while that of the active-material film was 80 nm. A set of four Al electrodes was deposited on top of the active material by thermal evaporation at $p < 5 \times 10^{-4}$ Pa. The light-emission area, as defined by the cathode-anode overlap, was 0.2 × 0.2 cm^2. The LECs were driven by a constant-current circuit and the voltage was logged by a microcontroller board (Arduino UNO) connected to a computer. The ITO electrode was invariably biased as the positive anode and Al was the negative cathode. The emitted radiance was measured with a calibrated Si photodiode (S2387-33R, Hamamatsu), and the emission spectrum was detected with a spectrometer (USB2000+, Ocean Optics). All of the above procedures, except for the deposition of the PEDOT:PSS layer, were carried out in two interconnected N_2-filled glove boxes ($[O_2] < 1$ ppm, $[H_2O] < 0.5$ ppm).

Supporting Information

Supporting Information is available from the Wiley Online Library or from the author.

Acknowledgements

The authors acknowledge financial support from the European Community's Seventh Framework Programme (FP7/2007-2013) under

Grant Agreement No. 607585 (OSNIRO), the Swedish Foundation for Strategic Research, Stiftelsen J.C. Kempes Minnes Stipendiefond, the Swedish Research Council, the Swedish Research Council Formas, the Swedish Energy Agency, the Wallenberg Foundation (2017.0186, 2016.0059), Stiftelsen Olle Engkvist Byggmastare, and Bertil & Britt Svenssons stiftelse för belysningsteknik. WM, ZG, and BAA gratefully acknowledge financial support from the International Science Programme, Uppsala University, Sweden. PM acknowledges funding from the Emil Aaltonen Foundation.

Conflict of Interest

The authors declare no conflict of interest.

Keywords

aggregation, energy transfer, light-emitting electrochemical cells, near-infrared emission, porphyrins

Received: October 2, 2020
Revised: December 1, 2020
Published online:

[1] a) E. C. Lee, H. Jung, D. Kim, *Sensors* **2011**, *11*, 2319; b) H. Suzuki, *J. Photochem. Photobiol., A* **2004**, *166*, 155; c) K. Liu, X. Liu, Q. Zeng, Y. Zhang, L. Tu, T. Liu, X. Kong, Y. Wang, F. Cao, S. A. G. Lambrechts, M. C. G. Aalders, H. Zhang, *ACS Nano* **2012**, *6*, 4054.

[2] A. Zampetti, A. Minotto, F. Cacialli, *Adv. Funct. Mater.* **2019**, *29*, 1807623.

[3] S. Strohm, F. Machui, S. Langner, P. Kubis, N. Gasparini, M. Salvador, I. McCulloch, H. J. Egelhaaf, C. J. Brabec, *Energy Environ. Sci.* **2018**, *11*, 2225.

[4] D. M. E. Freeman, A. Minotto, W. Duffy, K. J. Fallon, I. McCulloch, F. Cacialli, H. Bronstein, *Polym. Chem.* **2016**, *7*, 722.

[5] a) K. Tuong Ly, R.-W. Chen-Cheng, H.-W. Lin, Y.-J. Shiau, S.-H. Liu, P.-T. Chou, C.-S. Tsao, Y.-C. Huang, Y. Chi, *Nat. Photonics* **2016**, *11*, 63; b) E. Thimsen, B. Sadtler, M. Y. Berezin, *Nanophotonics* **2017**, *6*, 1043.

[6] U. Rösch, S. Yao, R. Wortmann, F. Würthner, *Angew. Chem., Int. Ed.* **2006**, *45*, 7026.

[7] a) S. Höfle, M. Pfaff, H. Do, C. Bernhard, D. Gerthsen, U. Lemmer, A. Colsmann, *Org. Electron.* **2014**, *15*, 337; b) T. B. d. Queiroz, M. B. S. Botelho, L. D. Boni, H. Eckert, A. S. S. d. Camargo, *J. Appl. Phys.* **2013**, *113*, 113508; c) G.-Y. Chen, B.-R. Chang, T.-A. Shih, C.-H. Lin, C.-L. Lo, Y.-Z. Chen, Y.-X. Liu, Y.-R. Li, J.-T. Guo, C.-W. Lu, Z.-P. Yang, H.-C. Su, *Chem. - Eur. J.* **2019**, *25*, 5489.

[8] a) Q. Pei, G. Yu, C. Zhang, Y. Yang, A. J. Heeger, *Science* **1995**, *269*, 1086; b) P. Matyba, K. Maturova, M. Kemerink, N. D. Robinson, L. Edman, *Nat. Mater.* **2009**, *8*, 672.

[9] A. Asadpoordarvish, A. Sandström, C. Larsen, R. Bollström, M. Toivakka, R. Österbacka, L. Edman, *Adv. Funct. Mater.* **2015**, *25*, 3238.

[10] a) A. Sandström, H. F. Dam, F. C. Krebs, L. Edman, *Nat. Commun.* **2012**, *3*, 1002; b) T. Lanz, A. Sandström, S. Tang, P. Chabrecek, U. Sonderegger, L. Edman, *Flexible Printed Electron.* **2016**, *1*, 025004; c) J. Zimmermann, L. Porcarelli, T. Rödlmeier, A. Sanchez-Sanchez, D. Mecerreyes, G. Hernandez-Sosa, *Adv. Funct. Mater.* **2018**, *28*, 1705795; d) J. Zimmermann, S. Schlisske, M. Held, J.-N. Tisserant, L. Porcarelli, A. Sanchez-Sanchez, D. Mecerreyes, G. Hernandez-Sosa, *Adv. Mater. Technol.* **2019**, *4*, 1800641.

[11] a) Z. Yu, X. Niu, Z. Liu, Q. Pei, *Adv. Mater.* **2011**, *23*, 3989; b) J. Liang, L. Li, X. Niu, Z. Yu, Q. Pei, *Nat. Photonics* **2013**, *7*, 817.

[12] Z. Zhang, K. Guo, Y. Li, X. Li, G. Guan, H. Li, Y. Luo, F. Zhao, Q. Zhang, B. Wei, Q. Pei, H. Peng, *Nat. Photonics* **2015**, *9*, 233.

[13] a) A. Sandström, A. Asadpoordarvish, J. Enevold, L. Edman, *Adv. Mater.* **2014**, *26*, 4975; b) P. Murto, S. Tang, C. Larsen, X. Xu, A. Sandström, J. Pietarinen, B. Bagemihl, B. A. Abdulahi, W. Mammo, M. R. Andersson, E. Wang, L. Edman, *ACS Appl. Energy Mater.* **2018**, *1*, 1753.

[14] A. Sandström, L. Edman, *Energy Technol.* **2015**, *3*, 329.

[15] a) G. Hernandez-Sosa, S. Tekoglu, S. Stolz, R. Eckstein, C. Teusch, J. Trapp, U. Lemmer, M. Hamburger, N. Mechau, *Adv. Mater.* **2014**, *26*, 3235; b) G. Mauthner, K. Landfester, A. Kock, H. Bruckl, M. Kast, C. Stepper, E. J. W. List, *Org. Electron.* **2008**, *9*, 164;

[16] a) S. Tang, A. Sandström, P. Lundberg, T. Lanz, C. Larsen, S. van Reenen, M. Kemerink, L. Edman, *Nat. Commun.* **2017**, *8*, 1190; b) P. Lundberg, Y. Tsuchiya, E. M. Lindh, S. Tang, C. Adachi, L. Edman, *Nat. Commun.* **2019**, *10*, 5307.

[17] a) H. J. Bolink, L. Cappelli, E. Coronado, P. Gaviña, *Inorg. Chem.* **2005**, *44*, 5966; b) H. J. Bolink, E. Coronado, R. D. Costa, P. Gaviña, E. Ortí, S. Tatay, *Inorg. Chem.* **2009**, *48*, 3907; c) W. Y. Ng, X. Gong, W. K. Chan, *Chem. Mater.* **1999**, *11*, 1165; d) X. Gong, P. K. Ng, W. K. Chan, *J. Nanosci. Nanotechnol.* **2002**, *2*, 151; e) H. Shahroosvand, L. Heydari, B. Nemati Bideh, B. Pashaei, *RSC Adv.* **2020**, *10*, 14099.

[18] a) A. R. Hosseini, C. Y. Koh, J. D. Slinker, S. Flores-Torres, H. D. Abruña, G. G. Malliaras, *Chem. Mater.* **2005**, *17*, 6114; b) D. A. W. Ross, P. A. Scattergood, A. Babaei, A. Pertegás, H. J. Bolink, P. I. P. Elliott, *Dalton Trans.* **2016**, *45*, 7748.

[19] B. Pashaei, S. Karimi, H. Shahroosvand, M. Pilkington, *Adv. Funct. Mater.* **2020**, *30*, 1908103.

[20] S. Xun, J. Zhang, X. Li, D. Ma, Z. Y. Wang, *Synth. Met.* **2008**, *158*, 484.

[21] C.-C. Ho, H.-F. Chen, Y.-C. Ho, C.-T. Liao, H.-C. Su, K.-T. Wong, *Phys. Chem. Chem. Phys.* **2011**, *13*, 17729.

[22] Y.-X. Liu, R.-H. Yi, C.-H. Lin, Z.-P. Yang, C.-W. Lu, H.-C. Su, *J. Mater. Chem. C* **2020**, *8*, 14378.

[23] H. Renner, G. Schlamp, I. Kleinwächter, E. Drost, H. M. Lüschow, P. Tews, P. Panster, M. Diehl, J. Lang, T. Kreuzer, A. Knödler, K. A. Starz, K. Dermann, J. Rothaut, R. Drieselmann, C. Peter, R. Schiele, J. Coombes, M. Hosford, D. F. Lupton, Platinum Group Metals and Compounds, in *Ullmann's Encyclopedia of Industrial Chemistry*, Wiley-VCH, Weinheim **2018**, https://doi.org/10.1002/9783527306732.a21_075.pub2.

[24] A. Pertegás, D. Tordera, J. J. Serrano-Pérez, E. Ortí, H. J. Bolink, *J. Am. Chem. Soc.* **2013**, *135*, 18008.

[25] S. Tang, P. Murto, X. Xu, C. Larsen, E. Wang, L. Edman, *Chem. Mater.* **2017**, *29*, 7750.

[26] D. Mauzerall, in *Photosynthesis I: Photosynthetic Electron Transport and Photophosphorylation*, Encyclopedia of Plant Physiology, Vol. *5* (Eds.: A. Trebst, M. Avron), Springer, Berlin **1977**, pp. 117–124.

[27] T. L. Poulos, *Chem. Rev.* **2014**, *114*, 3919.

[28] T. Virgili, D. G. Lidzey, D. D. C. Bradley, *Adv. Mater.* **2000**, *12*, 58.

[29] a) M. J. Plater, S. Aiken, G. Bourhill, *Tetrahedron* **2002**, *58*, 2415; b) A. Wiehe, C. Ryppa, M. O. Senge, *Org. Lett.* **2002**, *4*, 3807; c) G. Di Carlo, A. Orbelli Biroli, M. Pizzotti, F. Tessore, *Front. Chem.* **2019**, *7*, 177; d) Q. Arooj, G. J. Wilson, F. Wang, *RSC Adv.* **2016**, *6*, 15345.

[30] M. Mone, S. Tang, P. Murto, B. A. Abdulahi, C. Larsen, J. Wang, W. Mammo, L. Edman, E. Wang, *Chem. Mater.* **2019**, *31*, 9721.

[31] a) C. Bizzarri, E. Spuling, D. M. Knoll, D. Volz, S. Bräse, *Coord. Chem. Rev.* **2018**, *373*, 49; b) G. Cheng, G. K.-M. So, W.-P. To, Y. Chen, C.-C. Kwok, C. Ma, X. Guan, X. Chang, W.-M. Kwok, C.-M. Che, *Chem. Sci.* **2015**, *6*, 4623; c) Y. Hong, S. Chen, C. W. T. Leung, J. W. Y. Lam, J. Liu, N.-W. Tseng, R. T. K. Kwok, Y. Yu, Z. Wang, B. Z. Tang, *ACS Appl. Mater. Interfaces* **2011**, *3*, 3411.

[32] R. Kroon, A. Diaz de Zerio Mendaza, S. Himmelberger, J. Bergqvist, O. Bäcke, G. C. Faria, F. Gao, A. Obaid, W. Zhuang, D. Gedefaw,

E. Olsson, O. Inganäs, A. Salleo, C. Müller, M. R. Andersson, *J. Am. Chem. Soc.* **2014**, *136*, 11578.

[33] J. S. Lindsey, in *Metalloporphyrins Catalyzed Oxidations*, Catalysis by Metal Complexes (CMCO), Vol. *17* (Eds.: F. Montanari, L. Casella), Springer, Berlin **1994**, pp. 49–86.

[34] V. Pale, T. Nikkonen, J. Vapaavuori, M. Kostiainen, J. Kavakka, J. Selin, I. Tittonen, J. Helaja, *J. Mater. Chem. C* **2013**, *1*, 2166.

[35] B. Jia, H. Lian, T. Sun, H. Guo, X. Cheng, J. Wu, Y. Chen, Q. Dong, J. Huang, *Dyes Pigm.* **2018**, *159*, 298.

[36] Z. Li, X. Xu, W. Zhang, X. Meng, W. Ma, A. Yartsev, O. Inganäs, M. R. Andersson, R. A. J. Janssen, E. Wang, *J. Am. Chem. Soc.* **2016**, *138*, 10935.

[37] a) A. Zampetti, A. Minotto, B. M. Squeo, V. G. Gregoriou, S. Allard, U. Scherf, C. L. Chochos, F. Cacialli, *Sci. Rep.* **2017**, *7*, 1611; b) S. Baysec, A. Minotto, P. Klein, S. Poddi, A. Zampetti, S. Allard, F. Cacialli, U. Scherf, *Sci. China: Chem.* **2018**, *61*, 932; c) M. Sassi, N. Buccheri, M. Rooney, C. Botta, F. Bruni, U. Giovanella, S. Brovelli, L. Beverina, *Sci. Rep.* **2016**, *6*, 34096; d) O. Fenwick, J. K. Sprafke, J. Binas, D. V. Kondratuk, F. Di Stasio, H. L. Anderson, F. Cacialli, *Nano Lett.* **2011**, *11*, 2451; e) D.-H. Kim, A. D'Aléo, X.-K. Chen, A. D. S. Sandanayaka, D. Yao, L. Zhao, T. Komino, E. Zaborova, G. Canard, Y. Tsuchiya, E. Choi, J. W. Wu, F. Fages, J.-L. Brédas, J.-C. Ribierre, C. Adachi, *Nat. Photonics* **2018**, *12*, 98.

[38] a) Y. Pan, W. Li, S. Zhang, L. Yao, C. Gu, H. Xu, B. Yang, Y. Ma, *Adv. Opt. Mater.* **2014**, *2*, 510; b) H. Sun, Z. Hu, C. Zhong, X. Chen, Z. Sun, J.-L. Brédas, *J. Phys. Chem. Lett.* **2017**, *8*, 2393.

[39] A. Harriman, *J. Chem. Soc., Faraday Trans. 1* **1980**, *76*, 1978.

[40] N. M. de Amorim Lima, H. J. Camargo Avila, C. F. do Nascimento Marchiori, S. Gondim Sampaio, J. P. Ferreira Mota, V. Gomes Pereira Ribeiro, C. da Silva Clemente, G. Mele, M. Cremona, S. E. Mazzetto, *Materials* **2019**, *12*, 1063.

[41] C. Sandford, M. A. Edwards, K. J. Klunder, D. P. Hickey, M. Li, K. Barman, M. S. Sigman, H. S. White, S. D. Minteer, *Chem. Sci.* **2019**, *10*, 6404.

[42] a) S. Tang, P. Murto, J. Wang, C. Larsen, M. R. Andersson, E. Wang, L. Edman, *Adv. Opt. Mater.* **2019**, *7*, 1900451; b) W. Xiong, S. Tang, P. Murto, W. Zhu, L. Edman, E. Wang, *Adv. Opt. Mater.* **2019**, *7*, 1900280.

[43] S. Tang, H. A. Buchholz, L. Edman, *J. Mater. Chem.* **2015**, *3*, 8114.